

Communications

On the Adaptive Detection of Blood Vessels in Retinal Images

Di Wu, Ming Zhang, Jyh-Charn Liu, and Wendall Bauman

Abstract—This paper proposes an automated blood vessel detection scheme based on adaptive contrast enhancement, feature extraction, and tracing. Feature extraction of small blood vessels is performed by using the standard deviation of Gabor filter responses. Tracing of vessels is done via *forward detection*, *bifurcation identification*, and *backward verification*. Tests over twenty images show that for normal images, the *true positive rate* (TPR) ranges from 80% to 91%, and their corresponding false positive rates (FPR) range from 2.8% to 5.5%. For abnormal images, the TPR ranges from 73.8% to 86.5% and the FPR ranges from 2.1% to 5.3%, respectively. In comparison with two published solution schemes that were also based on the STARE database, our scheme has lower FPR for the reported TPR measure.

Index Terms—Adaptive contrast enhancement, blood vessel tracing, Gabor filter, retinal images.

I. ENHANCEMENT AND FEATURE EXTRACTION

Blood vessel detection needs to consider effects of lesions, pathological changes [1], and low contrast of small vessels [2]–[5]. In our scheme, the green channel of a color retinal fundus image is first inverted, and then its illumination is equalized by the scheme proposed in [6]. Next, the adaptive histogram equalization (AHE) technique proposed in [7] is modified by including a new parameter “ r ” as, $I_1(p) = \left(\sum_{p' \in R(p)} s(I(p) - I(p'))/h^2 \right)^r \cdot 255$, to enhance vessels, where $R(p)$ denotes the square window neighborhood with length h around a pixel p . $s(d) = 1$ if $d > 0$, and $s(d) = 0$ otherwise. Based on the performance measure $(\mu_v - \mu_b)/(\mu_v + \mu_b)$, it was found that the maximal contrast results from $h = 81$ and $r = 8$, where μ_v and μ_b represent the average intensity value of vessel pixels and that of background pixels, respectively.

In the enhanced image I_1 , both blood vessels (front layer) and some choroid (back layer) were highlighted [see Fig. 1(a)]. To differentiate these two types of objects, we developed a shape-based *Gabor standard deviation (GS) filter*, which is the standard deviation of the Gabor filter responses [8] along different directions on each pixel, where the Gabor filter is expressed by $g_\phi(u, v) = \exp(-\pi(u'^2/\sigma_u^2 + v'^2/\sigma_v^2)) \cos(2\pi fu')$, and $(u', v') = (u \cos \phi + v \sin \phi, -u \sin \phi + v \cos \phi)$.

Parameter setting of GS filter is derived from hand-traced vessel maps, which show the majority of vessel diameters are 3 pixels wide. Due to the significant differences in their textures, large blood vessels (wider than 3 pixels) and small vessels (3 pixels or less pixels wide) are detected using different features. Let $d = 3$. Following the procedure in [9], we get $f = 0.5/d$, $\sigma_u = n\lambda d/(0.75\pi)$ and $\sigma_v = 0.85\sigma_u$, for $n = 12$, and $\lambda = \sqrt{2 \ln 2/\pi}$. Filtering computation is truncated for $\sqrt{(x-u)^2 + (y-v)^2} > 1.5\sigma_u$.

Manuscript received April 13, 2004; revised May 1, 2005.

D. Wu and M. Zhang are with the Computer Science Department, Texas A&M University, College Station, TX 77843-3112 USA (e-mail: diwu8@cs.tamu.edu; mingz@cs.tamu.edu).

*J.-C. Liu are with the Computer Science Department, Texas A&M University, College Station, TX 77843-3112 USA (e-mail: liu@cs.tamu.edu).

W. Bauman is at 137 Primrose Place, San Antonio, TX 78209 USA.

Digital Object Identifier 10.1109/TBME.2005.862571

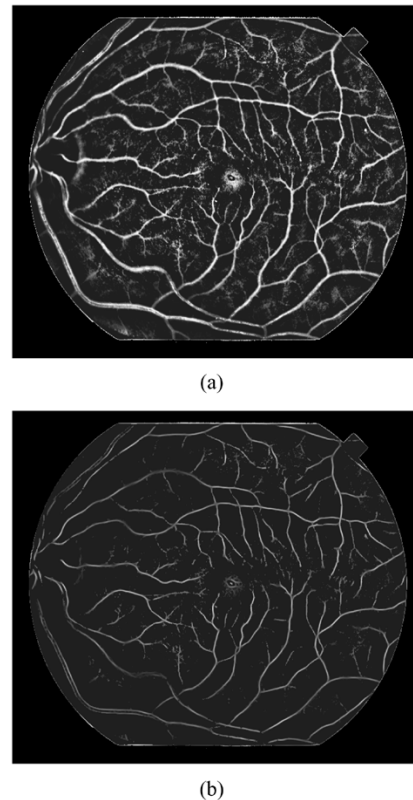


Fig. 1. (a) Contrast-enhanced map (I_1). (b) GS-filtering map (I_2).

The normalized GS filtering output (denoted as I_2) is illustrated in Fig. 1(b). The skeletons of small vessels are extracted with high contrasts, but I_2 is not effective for large vessels, i.e., some large vessels produce high GS responses on their centerlines or boundaries, yet others were shrunk, due to mismatched filter parameters. Nevertheless, large vessels can be readily detected in I_1 .

II. TRACING

The tracing subsystem is applied with the aid of the blood vessel feature maps (I_1 and I_2 , respectively, for large and small vessels) for precise detection of blood vessels. The initial points of the tracing algorithm are chosen by the following procedure: 1) In I_1 , a pixel is considered a candidate if it is located on a mesh grid and is between two consecutive edge points (identified by a Sobel detector) that have similar responses on opposite orientations. 2) In I_2 , local maxima points are selected as candidates, with the initial estimate of vessel width set to be d . 3) Candidates having local maxima of the *oriented feature response* (OFR) along two opposite directions are chosen as initial points, where OFR is essentially the Gaussian filter response of the vessels in I_1 (large vessels) or I_2 (small vessels.) That is, for large vessels

$$\text{OFR}_\theta(x, y) = \int \int_{H(x, y)} I_1(x-u, y-v) \xi_\theta(u, v) du dv \quad (1)$$

while for small vessels,

$$\text{OFR}_\theta(x, y) = \int \int_{H(x, y)} I_2(x-u, y-v) \xi_\theta(u, v) du dv \quad (2)$$

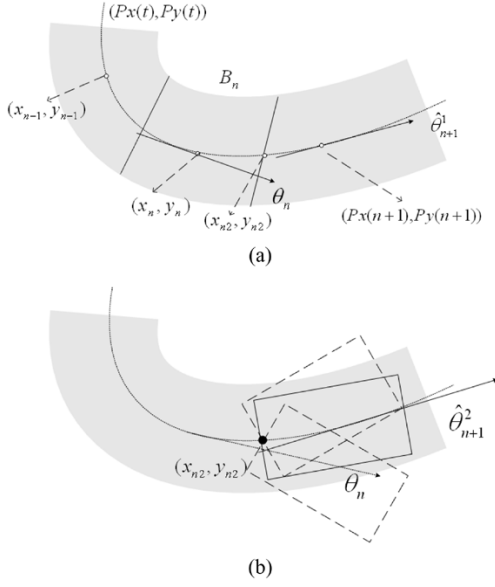


Fig. 2. Weighted-sum estimation of θ_{n+1} by (a) extrapolation and by (b) local greedy search.

where $\xi_\theta(u, v) = \exp(-\pi v'^2/\sigma^2)$ is a 2-D Gaussian filter oriented toward θ . The numerical convolution is done in the range of $H(x, y) = \{(u, v) : 0 \leq u' \leq 2w, |v'| \leq w\}$, where w is the vessel width, and $\sigma = 0.6w$. At each tracing run, the initial point with the largest vessel width is chosen to trace one new branch in segments, using *forward detection*, *bifurcation identification*, and *backward verification*, where the segment has the same width and length. Forward detection is based on an adaptive, weighted sum of the outcomes produced by *forward extrapolation* and *local greedy search* [see Fig. 2], as it is explained next.

Let B_1, \dots, B_n denote the n latest detected segments, where B_i is represented by its middle point (x_i, y_i) , width w_i , and direction θ_i . Forward extrapolation aims to predict the location and direction of B_{n+1} using B_1, \dots, B_n . The centerline of a vessel is approximated by a curve function $(P_x(t), P_y(t))$, which is comprised of two cubic splines constructed via interpolation on knots $\{(i, x_i)\}$ and $\{(i, y_i)\}$. The central point (x_{n+1}, y_{n+1}) of B_{n+1} is approximated by $(P_x(n+1), P_y(n+1))$. Let $\hat{\theta}_{n+1}^1$ denote the estimated θ_{n+1} , which is calculated by the tangential orientation of the curve function at $(P_x(n+1), P_y(n+1))$. Similarly, let \hat{w}_{n+1} denote the estimated w_{n+1} , which is calculated by the cubic spline at $(n+1, w_{n+1})$ that is constructed from interpolation on $\{(i, w_i)\}$.

At times, e.g., when the vessel has a sharp turn, $\hat{\theta}_{n+1}^1$ usually has a large prediction error. In this case, we use the local greedy search, which uses the strongest vessel feature along the current trajectory to predict the trajectory angle of B_{n+1} , i.e., $\hat{\theta}_{n+1}^2$, $\hat{\theta}_{n+1}^2 = \arg_\theta \max_{\theta \in (\theta_n - \Delta\theta, \theta_n + \Delta\theta)} \text{OFR}_\theta(x_{n2}, y_{n2})$. It is designed to offset prediction errors in $\hat{\theta}_{n+1}^1$, provided that $\text{OFR}_{\hat{\theta}_{n+1}^2}(x_{n2}, y_{n2}) > c_s \cdot \text{OFR}_{\theta_n}(x_n, y_n)$. (x_{n2}, y_{n2}) is the end point on the centerline of B_n , and $c_s = 0.5$ is set empirically. The angular range for prediction of the new segment is $\Delta\theta = 20^\circ$. The final prediction rule for θ_{n+1} is a weighted, adaptive decision rule $\hat{\theta}_{n+1} := c_p \cdot \hat{\theta}_{n+1}^1 + (1 - c_p) \cdot \hat{\theta}_{n+1}^2$. When the blood vessel curvature is less than 0.1 (no sharp turn), $c_p = 0.6$. Otherwise, c_p is set to be 0.4 (sharp turn detected.) Empirical results showed that this c_p value gave the best performance results [10], [11]. It worked well even in the presence of closely spaced blood vessels. Given $(P_x(n+1), P_y(n+1))$, $\hat{\theta}_{n+1}$ and \hat{w}_{n+1} , B_{n+1} is measured. On the *virtual* centerline specified by $(P_x(n+1), P_y(n+1))$ and $\hat{\theta}_{n+1}$,

TABLE I
PERFORMANCE OF OUR METHOD FOR 10 NORMAL (PATHOLOGY-FREE)
IMAGES AND 10 ABNORMAL (PATHOLOGICAL) IMAGES

Normal images		Abnormal images	
TPR (%)	FPR (%)	TPR (%)	FPR (%)
91.0	5.0	84.5	4.5
88.0	4.3	82.6	3.5
89.9	5.5	84.9	3.6
82.7	4.1	79.1	4.0
90.6	4.2	73.8	3.8
85.1	2.9	84.4	4.1
82.7	2.6	83.9	4.5
86.2	3.8	86.5	2.1
86.2	4.2	78.1	3.4
80.0	2.8	85.2	5.3

we look for two edges within the range of \hat{w}_{n+1} . The direction and centerline of B_{n+1} are then adjusted.

Bifurcation points are detected from the centerline of a vessel in the forward detection process. The detected bifurcation points are saved into the initialization list, so that they will be used as starting points for tracing on new branches. A bifurcation point is defined as the junction of three vessel branches, and the OFR along each of the three branches is relatively strong. A pixel on the centerline is considered a bifurcation point when three local maxima of its OFR values, OFR_{\max} , are detected along three different orientations. The pixel located at (x, y) has a local maximum of OFR along orientation θ' if

$$\text{OFR}_{\theta'}(x, y) = \max_{\theta} \text{OFR}_\theta(x, y) \quad \theta \in [\theta' - \Delta\theta, \theta' + \Delta\theta] \quad (3)$$

and

$$\text{OFR}_{\theta'}(x, y) \geq \mu_{\text{OFR}}(x, y) + C_b \cdot \sigma_{\text{OFR}}(x, y) \quad (4)$$

where $c_b > 0$ is a constant, $\mu_{\text{OFR}}(x, y)$ and $\sigma_{\text{OFR}}(x, y)$ are, respectively, the average and standard deviation of the OFRs along all discretized orientations. Equation (4) is designed to eliminate false detections. $c_b = 0.7$ suffices when the angular resolution is 10° .

The backward verification process uses vessel widths and OFR values of adjacent segments for outlier detection using *critical values* in [12]. In this simple process, $Z = |x - \bar{x}|/std$ was first calculated, where x is the sample being examined, and \bar{x} and std are, respectively, the mean and standard deviation of the observations. An outlier is detected when the test outcome of x exceeds the critical value. Experimental results show that this scheme is highly effective in eliminating false detections that would be caused by lesions or hemorrhages located next to vessels or bifurcation points.

III. EXPERIMENTAL RESULTS AND SUMMARY

One normal image and one abnormal image in the STARE database [1] were randomly chosen and used for training the parameters. The other eighteen retinal images in STARE were tested, using their (first set of) hand-labeled vessel maps as ground truth, and the *true positive rate* (TPR) and *false positive rate* (FPR) [1] as performance criteria. The TPR and FPR values for the twenty images are given in Table I, and the overall average performance is 84.3% for TPR, and 3.9% for FPR. A further study shows that 75% of small vessels were captured, where small vessels account for 42% of vessel pixels.

The majority of large and small vessels were detected, see Fig. 3 for an example. Most false detections are due to incorrectly identified initial tracing points. For comparison, the multithreshold probing method [13] will need to increase its FPR to 5% to achieve the same level of TPR as ours, and the filter response analysis method [1] needs to increase its FPR value significantly to achieve the same goal. Our scheme requires very

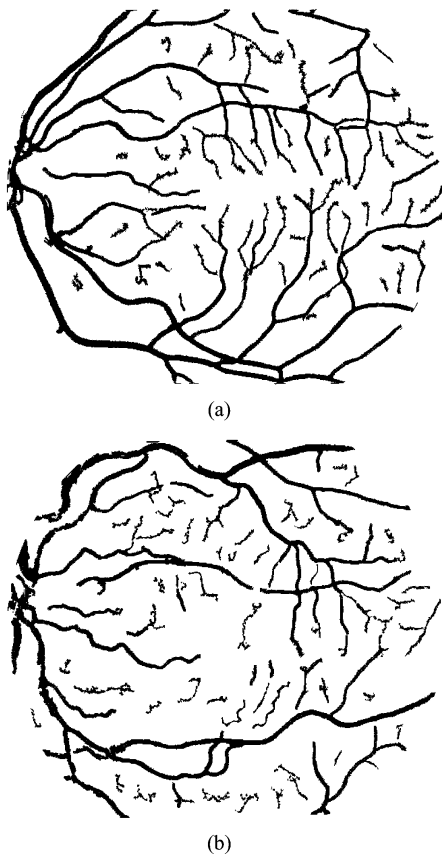


Fig. 3. Detection results of one normal image (0077) and one abnormal image (0001).

little calibration. In contrast, the two approaches that are being compared need eight and ten sets of parameter values, respectively.

REFERENCES

- [1] A. Hoover, V. Kouznetsova, and M. Goldbaum, "Locating blood vessels in retinal images by piecewise threshold probing of a matched filter response," *IEEE Trans. Med. Imag.*, vol. 19, no. 3, pp. 203–210, Mar. 2000.
- [2] A. Can, H. Shen, J. N. Turner, H. L. Tanenbaum, and B. Roysam, "Rapid automated tracing and feature extraction from retinal fundus images using direct exploratory algorithms," *IEEE Trans. Inf. Technol. Biomed.*, vol. 3, no. 2, pp. 125–138, Jun. 1999.
- [3] L. Zhou, M. Rzeszotarski, L. Singerman, and J. Chokreff, "The detection and quantification of retinopathy using digital angiograms," *IEEE Trans. Med. Imag.*, vol. 13, no. 4, pp. 619–626, Dec. 1994.
- [4] O. Chutatape, L. Zhang, and S. M. Krishnan, "Retinal blood vessel detection and tracking by matched Gaussian filter and Kalman filters," in *Proc. 20th Int. Conf. IEEE Engineering in Medicine and Biology Society*, vol. 6, Hong Kong, China, 1998, pp. 3144–3149.
- [5] L. Gang, O. Chutatape, and S. Krishnan, "Detection and measurement of retinal vessels in fundus images using amplitude modified second-order Gaussian filter," *IEEE Trans. Biomed. Eng.*, vol. 49, no. 2, pp. 168–172, Feb. 2002.
- [6] A. Hoover and M. Goldbaum, "Locating the optic nerve in a retinal image using the fuzzy convergence of the blood vessels," *IEEE Trans. Med. Imag.*, vol. 22, no. 8, pp. 951–958, Aug. 2003.
- [7] J. A. Stark, "Adaptive image contrast enhancement using generalizations of histogram equalization," *IEEE Trans. Image Process.*, vol. 9, no. 5, pp. 889–896, May 2000.
- [8] J. G. Daugman, "Uncertainty relation for resolution in space, spatial frequency and orientation optimized by two-dimensional visual cortical filters," *J. Opt. Soc. Am.*, vol. 2, pp. 1160–1169, Jul. 1985.
- [9] Z.-Q. Liu, J. Cai, and R. Buse, *Handwriting Recognition: Soft Computing and Probabilistic Approaches*. Berlin, Germany: Springer-Verlag, 2003.
- [10] D. Wu, M. Zhang, J. C. Liu, and W. Bauman, "On the Adaptive Detection of Blood Vessels in Retinal Images," Dept. Comput. Sci., Texas A&M Univ., College Station, TX, Tech. Rep. 2005-3-3, 2005.
- [11] D. Wu, "Segmentation, registration, and selective watermarking of retinal images," Ph.D. dissertation, Dept. Comput. Sci., Texas A&M Univ., College Station, TX, 2005.
- [12] F. Grubbs, "Procedures for detecting outlying observations in samples," *Technometrics*, vol. 11, no. 1, pp. 1–21, Feb. 1969.
- [13] X. Jiang and D. Mojon, "Adaptive local thresholding by verification-based multithreshold probing with application to vessel detection in retinal images," *IEEE Trans. Pattern Anal. Mach. Intell.*, vol. 25, no. 1, pp. 131–137, Jan. 2003.

Comparison of Atrial Signal Extraction Algorithms in 12-Lead ECGs With Atrial Fibrillation

Philip Langley*, José Joaquín Rieta, Martin Stridh, José Millet, Leif Sörnmo, and Alan Murray

Abstract—Analysis of atrial rhythm is important in the treatment and management of patients with atrial fibrillation. Several algorithms exist for extracting the atrial signal from the electrocardiogram (ECG) in atrial fibrillation, but there are few reports on how well these techniques are able to recover the atrial signal. We assessed and compared three algorithms for extracting the atrial signal from the 12-lead ECG.

The 12-lead ECGs of 30 patients in atrial fibrillation were analyzed. Atrial activity was extracted by three algorithms, Spatiotemporal QRST cancellation (STC), principal component analysis (PCA), and independent component analysis (ICA). The amplitude and frequency characteristics of the extracted atrial signals were compared between algorithms and against reference data.

Mean (standard deviation) amplitude of QRST segments of V1 was 0.99 (0.54) mV, compared to 0.18 (0.11) mV (STC), 0.19 (0.13) mV (PCA), and 0.29 (0.22) mV (ICA). Hence, for all algorithms there were significant reductions in the amplitude of the ventricular activity compared with that in V1. Reference atrial signal amplitude in V1 was 0.18 (0.11) mV, compared to 0.17 (0.10) mV (STC), 0.12 (0.09) mV (PCA), and 0.18 (0.13) mV (ICA) in the extracted atrial signals. PCA tended to attenuate the atrial signal in these segments. There were no significant differences for any of the algorithms when comparing the amplitude of the reference atrial signal with that of the extracted atrial signals in segments in which ventricular activity had been removed. There were no significant differences between algorithms in the frequency characteristics of the extracted atrial signals. There were discrepancies in amplitude and frequency characteristics of the atrial signal in only a few cases resulting from notable residual ventricular activity for PCA and ICA algorithms.

Manuscript received October 7, 2004; revised May 8, 2005. This work was supported in part by the Spanish Council under Grant TIC2002-00957 and Grant IARC0/2004/249 Generalitat Valenciana. The work of P. Langley was supported in part by the UK Engineering and Physical Sciences Research Council under Grant GR/R37890/01. Asterisk indicates corresponding author.

*P. Langley is with the Cardiovascular Physics and Engineering Research Group, Medical Physics Department, Freeman Hospital, University of Newcastle upon Tyne, Newcastle upon Tyne NE7 7DN, U.K. (e-mail: philip.langley@ncl.ac.uk).

J. J. Rieta and J. Millet are with the Bioengineering Electronic and Telemedicine Research Group, Electronic Engineering Department, Polytechnic University of Valencia. EPSG, Carretera Nazaret Olivia s/n, 46730, Gandia, Valencia, Spain.

M. Stridh and L. Sörnmo are with the Signal Processing Group, Department of Electrosience, Lund University, SE 221 00 Lund, Sweden.

A. Murray is with the Cardiovascular Physics and Engineering Research Group, Medical Physics Department, Freeman Hospital, University of Newcastle upon Tyne, Newcastle upon Tyne NE7 7DN, U.K.

Digital Object Identifier 10.1109/TBME.2005.862567